APPLICATION OF SATELLITE IMAGES TO LOCATE AND INVENTORY VINEYARDS IN THE DESIGNATION OF ORIGIN "BIERZO" IN SPAIN

J. R. Rodríguez, D. Miranda, C. J. Álvarez

ABSTRACT. *With a view to contributing to the improvement of the current vineyard registers, this study presents a methodology for vineyard mapping based on satellite remote sensing systems. The procedure was validated for the Designation of Origin "Bierzo" in Spain. Different supervised classifications were performed based on two Landsat images acquired in the same year. The objectives of the present study were to determine which classification yielded the best results and to quantify the influence of different factors that affected the overall classification accuracy, such as the resampling method, the use of georeferenced mosaics, or the combination of the two images. The classification accuracy was determined by using confusion matrices that were applied to two ground truth images: one of the images consisted of a 700 × 700 m pixel grid, and another image was generated from validation sites. The percentages of agreement obtained exceeded 75%. Based on the results obtained, the area under vines at the municipal level was estimated by linear regression. A strong correlation (R > 0.84) was observed between the official statistical data and the data obtained from image classifications.*

Keywords. *Landsat TM, Remote sensing, Vineyard registers, Vineyards.*

Remote sensing techniques have enabled the development of many applications related to vines. In the last few years, the progression has been so strong that up to 18 variables that affect vineyard productivity have been identified using multispectral image data (Franson, 2001; Hall et al., 2002). Research in this field began in the mid-1980s and was oriented towards classification of land uses and quantification of erosion problems. In the 1990s, new research lines were developed to detect stress problems in vines by using hyperspectral images. The most recent applications have focused on precision viticulture, and on grapevine environment modeling for integrated crop management.

Remote sensing vineyard identification presents some problems that must be overcome. The land cover of vineyards is discontinuous (the soil surface is not completely covered) because vines are planted at a specific spacing. Therefore, the soil pattern has a remarkable influence on the image. The arrangement of vines requires the use of high spatial resolution sensors that entail a high economic cost. However, some authors have obtained good results using medium spatial resolution images (Tsiligirides, 1998). The results of this type of research are strongly influenced by local conditions. Although it is possible to determine the spectral response for the typical vineyard, this response is largely affected by the physicochemical properties of soil (Arán et al., 2001).

One of the first research works that classified vineyards using Landsat imagery was carried out in the state of New York (Troiler et al., 1989), but the results obtained were not as satisfactory as initially expected. Another approach to the problem of vineyard identification consists of conducting multitemporal studies or combining bands of multispectral images. In this way, good results have been obtained with TM (Landsat 5) using masking classification methods (Lanjeri, 1998; Lanjeri et al., 2001a). The improvements achieved in the studies mentioned consisted of classifying the different land uses in successive stages: rainfed crops were extracted by principal component analysis; fallow, forest, and olive land uses were extracted by using supervised classifications of an image acquired in May; irrigated crops, urban areas, and ponds were extracted by using a supervised classification; and the rest of the surface was considered as vineyard. Each step in the process consisted of generating a mask for each discriminated cover. The generated mask removed the classified pixels from the image.

Another classification technique is based on identifying the combinations of bands that optimize the separability between vines and the rest of the crops (Rubio et al., 2001a, 2001b). This classification technique has been validated with an accuracy of 91% for vineyards located in Tomelloso, Ciudad Real, Spain. The validated technique can be improved by using images from different seasons.

In Portugal, remote sensing systems have been used to map vineyards (Bessa, 1994). The project developed a methodology for defining the area under vines from Landsat images and color-infrared photographs. Such information was included in a Geographical Information System (GIS)

Article was submitted for review in January 2005; approved for publication by the Information & Electrical Technologies Division of ASABE in November 2005.

The authors are **José R. Rodríguez,** Associate Professor, Escuela Superior y Técnica de Ingeniería Agraria, University of León, León, Spain; **David Miranda,** Assistant Professor, and **Carlos J. Álvarez,** Associate Professor, Department of Agroforestry Engineering, University of Santiago de Compostela, Lugo, Spain. **Corresponding author:** Carlos J. Álvarez, University of Santiago de Compostela, Escola Politécnica Superior, Campus Universitario s/n, 27002 Lugo, Spain; phone: +34-98225-2231; fax: +34-98228-5926; e-mail: proyca@lugo.usc.es.

  ISSN 0001−2351

together with data of the physical environment (topography, petrology, climatology, etc.). The data obtained were integrated with the analysis capabilities of GIS.

In the same research line, some authors have studied crop evolution during a given period. The main objective of their research was to assess the effects of the Common Agricultural Policy of the European Union (Lanjeri et al., 2001b; García and García, 2001). Other authors have used active sensors, such as radar, to classify vineyards (Company et al., 1994; Bugden et al., 1999). Good results were obtained with these sensors: vineyards were classified with an accuracy of 80%. However, these systems are expensive and very sensitive to vine training system (spur prune, cordon training, trellis training, etc.).

Until now, the best results have been obtained by applying techniques based on the Fourier transform to high-resolution color aerial photographs (Robbez-Masson et al., 2001; Wassenaar et al., 2001) and color-infrared aerial photographs (Ranchin et al., 2001). By using these techniques, vines can be identified from regular planting because the techniques analyze the repetition of patterns such as form, texture, and orientation of vines, rather than the spectral response of vines. The main advantage of using this group of classifiers is the achievement of certain automation of the process (Escalera, 2001).

In Spain, research projects concerned with remote sensing of vineyards are currently being developed. The European Union has funded the project titled "Methodological approach for vineyard inventory and management (BACCHUS)," carried out between 2003 and 2005 in Castilla-La Mancha, central Spain. The aim of the project was to develop a remote sensing based methodology to inventory and manage vineyards, which was validated for the study area.

European Union of the Council Regulation (EC) No. 1493/1999 on the common organization of the market in wine, dated 17 May 1999, established that the member states should have reliable and updated information about wine-producing holdings, vine-growing areas, and wine produced. The regulation established the need to compile a regional inventory of wine production.

In Spain, vineyard registers already exist. Act 25/1970 established the first Vineyard Register. The former National Institute of Designations of Origin (Instituto Nacional de Denominaciones de Origen − INDO) compiled a National Vineyard Register composed of graphic and alphanumeric databases. Moreover, the Orders of 23 May 1986 and 18 July 1998 of the Regional Ministry of Agriculture, Farming and Forestry of the autonomous community of Castilla y León established the creation of a register of vineyards and replanting rights in this community, in which the present study was conducted. However, the registers are currently outdated, and the compilation of a new Vineyard Register with updated land references has been considered necessary. With the compilation of the new register, all the areas under vines in Castilla y León have been regularized pursuant to Regulation (EC) No. 1493/1999.

Vineyard Registers currently use information from the official agricultural censuses conducted by the Spanish Ministry of Agriculture every ten years. The latest agricultural census was conducted in 1999. The data contained in the agricultural censuses are gathered from interviews with all the farm owners, who provide information about areas, crops, types of land use, and other socioeconomic variables. Based on this information, a given number of farms are selected and field sampling is conducted every three years in order to anticipate modifications of census data. However, preliminary surveys are usually expensive, are not systematic, and lack thorough quality control. Consequently, a new methodology is required to avoid such problems.

Objectives

The objective of this study is to present a methodology for mapping vineyards from satellite imagery, and to validate the methodology. This methodology aims to be useful in the development and management of Vineyard Registers, and to contribute in a reliable and cost-effective manner to the estimation of the area under vines at the municipal level (Rodríguez, 2003).

The research work was divided into two well-differentiated stages: (1) determination of the most efficient classification method to identify vineyards, and (2) quantification of the vineyard area in El Bierzo.

Materials and Methods

The region of El Bierzo, with an area of approximately 3000 km^2, is located to the northwest of the Autonomous Community of Castilla y León, Spain. The study area covers the municipalities that compose the Designation of Origin Bierzo, which accounts for an area of 1,410.07 km^2 (fig. 1).

This zone satisfies the degree of variability required because it shows a high level of fragmentation of crops, soils, and topography. Moreover, the results obtained for this region can be extrapolated to other wine-producing areas because the study area is sufficiently large.

According to the data gathered from official statistics and from the Regulating Cabinet, the vineyards in El Bierzo present the following characteristics:

- High fragmentation level, which involves a very small vineyard size (the average size of plots is 0.2 ha). Fragmentation is an important structural limitation for the application of new cultivation techniques.
- Low professionalization, which causes delay in the implementation of new cultivation techniques. Wine-producing holdings are managed by non-professional vine

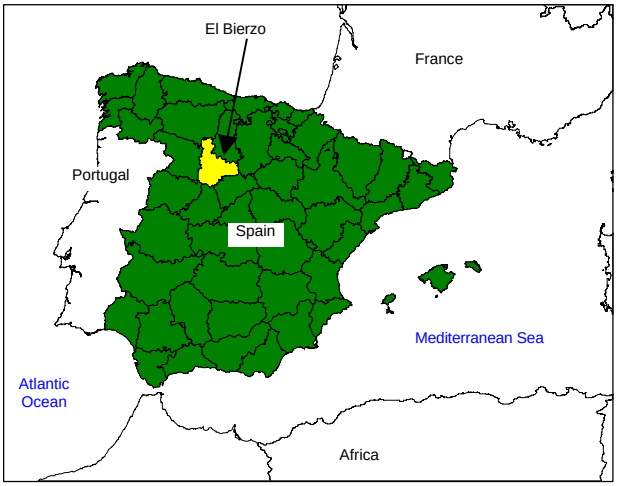

Figure 1. Location of the region of El Bierzo, Autonomous Community of Castilla y León, Spain.

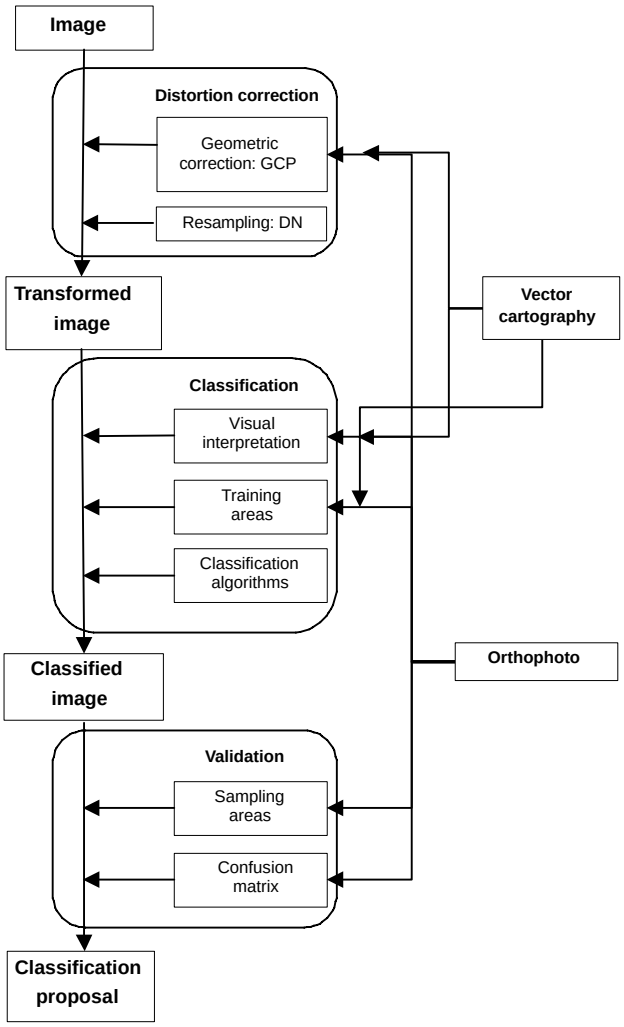

Figure 2. Methodological process developed for image classification.

growers or part-time farmers who consider that the aim of the wine-producing holding is productivity and do not take into consideration criteria to improve the quality of grapes.

- Investment in research, development, and innovation in viticulture is limited to grants from the Regional Administration for vineyard renovation.

Our research was based on two Landsat (TM and ETM+) images of the study area, acquired at two different times (June and September 2000). In addition, digital cartography (with spatial resolution at 1:10000 scale) and color orthophotos (0.7 m^2 pixels) acquired between September and October 2000 were used to georeference the satellite images. Color orthophotos were used to define the areas for training and validating the results of the classifications.

With regard to software, ENVI was used to visualize and process images. IDRISI version R.02 was used for management and analysis of georeferenced data and for digital processing of images. AutoCAD, particularly the Autodesk Map tool, was used to generate topologies, store drawing data in an Oracle Spatial database, import cartographic data from other CAD and GIS systems, link maps to associated databases, and manage, extract, and store graphic and alphanumeric data. Other software packages such as ArcView, ECW Header Editor, ERViewer 2.0c, ECW Compressor 2.3 (www.ermapper.com), and MicroStation (Bentley) were also used. Figure 2 summarizes the methodological process developed in this study.

This methodological process consisted of the following five phases, which are explained in detail in the following sections:

1. Pre-processing of the images for correction of geometric distortions.
2. Classification of each image using different algorithms in order to determine which algorithm yields the best results in the study area.
3. Quantification of the effects of different factors on the classification: pixel resampling method, differences between using images with the digital number values and calibrated images, and contribution of thermal bands.
4. Combination of the two classified images (acquired in June and September) to improve the results obtained from the initial classifications.
5. Estimation of the area under vines based on the classifications obtained by correlating the results with statistical data at the municipal level.

Phase 1: Pre-Processing of the Images

The images acquired in different seasons were geometrically corrected and georeferenced before classification. Correction of geometric distortions consists of modifying pixel location and allows transformation of images into cartographic projections with minimum digital number (DN) changes (Lillesand and Kiefer, 1994). Transformations are based on numerical functions that assign a new location to each pixel according to the input matrix or vector coordinates. Digital format makes process automation easier.

The mathematical formulation of geometric corrections is expressed as (Chuvieco, 2002; Pinilla, 1995):

$$u = f_1(x, y) = f_2(c, l)$$

$$v = g_1(x, y) = g_2(c, l) \quad (1)$$

where (x, y) are the vector coordinates of the pixel, (c, l) are the column-row matrix coordinates, and (u, v) are the corrected coordinates.

The most common methods for geometric correction of images are: (1) correction using the orbital model, and (2) correction using ground control points (GCPs), which was the empirical procedure used in this research. GCP coordinates were determined from digital orthophotos and vector maps, and were assigned to the corresponding pixel (column, row). Therefore, the acquisition of coordinates was based on orthophotos, from which a mosaic was generated.

With regard to spectral analysis, an initial assessment was conducted by determining the basic statistical parameters (means, extreme values, and standard deviation).

Phase 2: Classification of Images using Different Algorithms

An initial visual interpretation was carried out by producing different color composites, which verified the high degree of heterogeneity of the land cover in the area. The complexity of the tessellation became more evident in vineyard areas due to the small size of the plots. Moreover, many vineyards were abandoned during the last few years,

and visual detection of the areas covered by vines became difficult because of the spatial resolution of the TM sensor (30 m).

The definition of the land cover types to be discriminated and of the training areas was based on visual interpretation of images, orthophotos (a total of 85), and field visits and surveys performed across the municipalities included in the study area. An unsupervised classification was conducted in order to guarantee the statistical distinction between the cover types. In this classification, a maximum of 30 classes were initially defined, with a change threshold of 5% and a minimum class size of 50 pixels.

To select the land covers to discriminate, previous studies were considered (Rodríguez et al., 2002), in addition to the most representative covers and other less common covers that must be differentiated from vines. Although 38 classes were initially identified, the validation of results required reorganization of the discriminated cover types.

Four different classification algorithms were used to classify the images: maximum likelihood (with a likelihood threshold of 80%), parallelepiped classification (with a maximum standard deviation of 3.00), minimum distance (with the same value as the previous algorithm), and Mahalanobis distance (without restrictions). These classification algorithms are explained below. In previous studies with similar images, the best classifications were obtained by using the maximum likelihood algorithm (Rodríguez et al., 2002; Martínez et al., 2002).

Maximum Likelihood Classification

The maximum likelihood algorithm is a direct application of the Bayesian decision theory. This method calculates the probabilities that a pixel belongs to each possible class and assigns the pixel to the most likely class. The maximum likelihood algorithm assumes that the class histograms are normally distributed (RSI, 2000).

Assuming a normal distribution of DNs within each class, a probability function can be used to describe each category according to the mean vector and variance-covariance matrix of the category, in order to determine the probability that a pixel belongs to a particular class. The calculation is performed for each category involved in the classification, and the pixel is assigned to the category that maximizes the probability function (Gibson and Power, 2000).

Normal distribution functions are previously calculated for each class using the mean and variance values obtained in training areas, and each pixel is assigned (as a function of DN) to the most likely class. Considering only one band of an image, the probability that a pixel with a value z belongs to a particular class is quantified by:

$$p(z/C_i) = \frac{1}{\sigma_i\sqrt{2\pi}} e^{-\frac{1}{2}\left(\frac{z-\mu_i}{\sigma_i}\right)^2} \quad (2)$$

where μ_i and σ_i are the parameters that characterize C_i. For a total of n classes, it can be concluded that the pixel belongs to C_i if the following expression is verified:

$$p(z/C_i) \geq p(z/C_j)$$

$$\forall\ i \neq j;\ \ j = 1, 2, \ldots n \quad (3)$$

It is generally assumed that the probabilities for all the classes are equal. However, if we know that this condition is not fulfilled, then we can specify weighting factors for each class that implement the different probabilities in the expression. Such factors can be considered as weights that are incorporated into the expression:

$$p(z/C_i)\,p(C_i) \geq p(z/C_j)\,p(C_j)$$

$$\forall\ i \neq j;\ \ j = 1, 2, \ldots n \quad (4)$$

where $p(C_i)$ and $p(C_j)$ are the *a priori* probabilities for each class.

Determining values for the weighting factors is not easy. A commonly used criterion consists of assigning a probability to each class that is proportional to the area covered by that class in the study area. However, the determination of such probability is not easy without knowledge of the area (Eastman, 1999). Figure 3 shows, in one dimension, the effect of changing the *a priori* probability of a class.

In addition, probability thresholds can be established for each class so that the elements whose maximum probability of belonging to a class is lower than the threshold established for that class remain unclassified (fig. 4). If the number of unclassified pixels is high, either the training areas must be redefined or the probability threshold must be lowered *a posteriori*.

The maximum likelihood algorithm is the most complex classifier and demands a large number of calculations. However, it is the most widely used algorithm in remote sensing because it is robust and fits the arrangement of original data more strictly (Chuvieco, 2002).

Parallelepiped Classification

In the parallelepiped method, a decision region is defined for each class based on the highest and lowest values of each

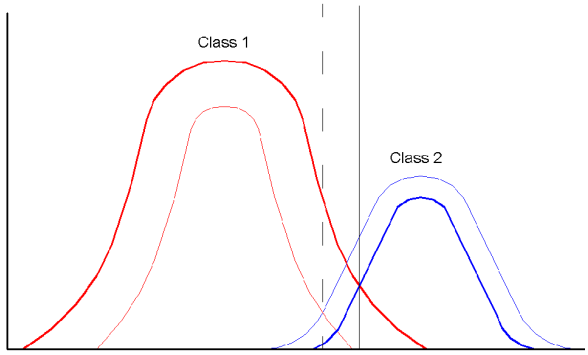

Figure 3. Maximum likelihood classification.

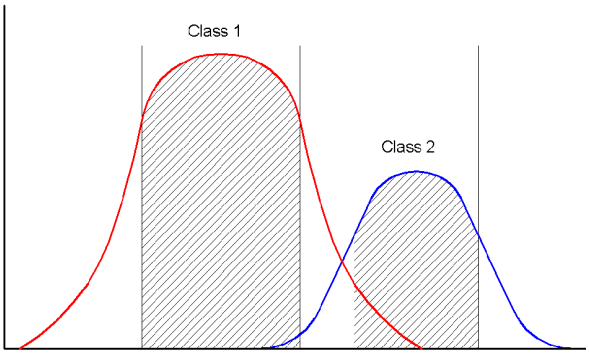

Figure 4. Definition of probability thresholds.

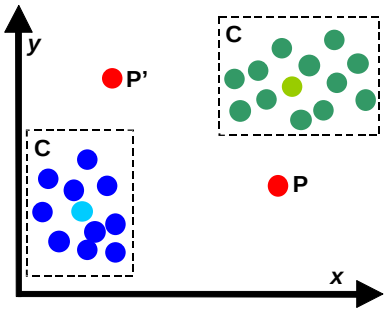

Figure 5. Parallelepiped classification method.

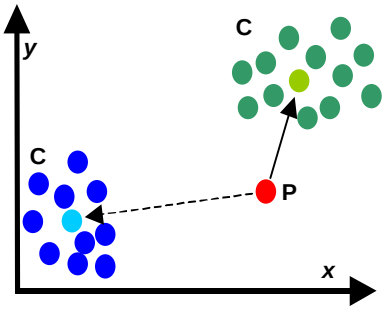

Figure 6. Minimum-distance classification method.

class. Some modifications of this method establish other limits based on the central tendency and dispersion of values. The geometric shape of the area is a parallelepiped that defines each region in the *n*-dimensional pattern space (fig. 5).

As shown in figure 5, a pixel belongs to a particular class if it lies in the parallelepiped defined by that class. Consequently, a pixel with a digital number value of DN(*k*) in band *k* of the *n* bands that compose the image is assigned to class *C* if the following expression is verified (Pinilla, 1995):

$$\overline{DN}_C(k) - R_C(k) < DN_C(k) < \overline{DN}_C(k)_C + R_C(k)$$

$$\forall 1 \le k \le n \qquad (5)$$

where R_C is the dispersion range around the mean value. Although the dispersion range is established by the analyst, it usually corresponds to standard deviation or some multiple of standard deviation (Chuvieco, 2002).

The parallelepiped classifier is a fast and simple method that requires little sample information. However, this method has two main drawbacks: some pixels may remain unclassified (such as *P* and *P'* in fig. 5), and some parallelepipeds may overlap. The problem of overlapping parallelepipeds is usually solved by assigning the pixel to the first class identified or to the class with the minimum Euclidean distance.

Minimum Distance Classification

Minimum distance classification assigns the unknown pixel to the category that minimizes the distance between the pixel and the class centroid (fig. 6). Distance must be understood as spectral distance, not geographical distance. The centroid of a class can be defined as a vector whose components are the average sample values of the pixels in each band for that class. Euclidean distance is used to compute the distance between the pixel and the class centroid, according to the expression:

$$d_C = \sqrt{\sum_{i=1}^{n} (DN_i - \overline{DN}_{Ci})^2} \qquad (6)$$

Therefore, the distance between the pixel and the class centroid is computed as the square root of the sum for all the bands of the squares of the difference between the digital number of the cell (DN_i) and the average of the digital numbers of the cells that compose class C_i (Pinilla, 1995).

Generally, a threshold is defined for each class in order to establish the maximum distance at which a pixel can be assigned to a given class. As a result, maximum distances are parameterized for each class according to the degree of pixel clustering. This procedure is simple and fast, but insensitive to class variability and dispersion.

Mahalanobis Distance Classification

Mahalanobis distance classification improves minimum distance classification. Mahalanobis distance assumes that the histograms of the classes are normally distributed and that the scatter diagram representing the set of pixels assigned to a class has the shape of an ellipsoid. Figure 7 shows the shape of the scatter diagram for two bands. The ellipsoidal shape of the diagram depends on the mean, variances, and covariances of data.

Mahalanobis distance is sensitive to class variability. For example, when classifying urban areas, which are largely variable, this method can correctly classify "urban" pixels that are closer to the centroid of the "water" class, whose values are more clustered and show lower variance. Figure 7 illustrates this example. Using minimum distance classification, point *P* would have been assigned to class C_2. However, the intrinsic nature of the correlation between the pixels in each class suggests that point *P* actually belongs to C_1. The Mahalanobis distance method is sensitive to this consideration. The Mahalanobis distance is computed for each class according to the following expression:

$$d_M = \sqrt{(\vec{z} - \vec{\mu})^t \, \Sigma^{-1} (\vec{z} - \vec{\mu})} \qquad (7)$$

where $\vec{z}$ is the matrix of digital numbers (vector of data), $\vec{\mu}$ is the matrix of mean values (mean vector), and Σ^{-1} is the inverse of the covariance matrix.

Phase 3: Quantification of the Effects of Different Factors on the Classification

In regard to DN resampling, the use of transformation functions enables correction of the image position, but it is necessary to transfer DNs in each band. Such operation is termed resampling and is used to obtain the transformed

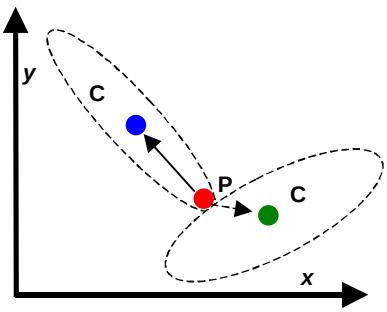

Figure 7. Mahalanobis distance.

image from the corrected image. Resampling is a complex process because each pixel of the new image is surrounded by several pixels of the original image. This problem becomes more serious when the geometric resolution is altered during image transformation.

DN transfer can be performed according to different methods, such as nearest neighbor resampling, bilinear interpolation, or cubic convolution. Nearest neighbor resampling does not alter the DNs of the original image, while bilinear interpolation and cubic convolution interpolate original DNs (Pinilla, 1995).

With the nearest neighbor method, each pixel of the corrected image is assigned the value of the nearest pixel in the original image. Nearest neighbor resampling is rapid and does not alter original DNs. However, it introduces distortions in linear elements. This method can be algebraically expressed as:

$$f(c,l) \begin{cases} f(x,y) & \Delta x < 0{,}5 \quad \Delta y < 0{,}5 \\ f(x+1,y) & \Delta x \geq 0{,}5 \quad \Delta y < 0{,}5 \\ f(x,y+1) & \Delta x < 0{,}5 \quad \Delta y \geq 0{,}5 \\ f(x+1,y+1) & \Delta x \geq 0{,}5 \quad \Delta y \geq 0{,}5 \end{cases} \tag{8}$$

where $f(c, l)$ is the digital number assigned to cell (c, l) of the corrected image; Δx and Δy are the differences in row and column direction between the center of the corrected pixel and the center of the transformed pixel, expressed in fractions of a pixel; and $f(x, y)$ is the value of the transformed image pixel, located in a position defined by a real number, where:

$$\begin{aligned} c &= x + \Delta x \qquad 0 \leq \Delta x \leq 1 \\ l &= y + \Delta y \qquad 0 \leq \Delta y \leq 1 \end{aligned} \tag{9}$$

Bilinear interpolation finds the average of the DNs of the four nearest pixels in the original image. The computed average is weighted according to the distance between the original pixel and the corrected pixel (Chuvieco, 2002). This method avoids distortions in linear elements but reduces the spatial contrast in the image. The mathematical formulation of bilinear interpolation can be expressed as:

$$\begin{aligned} f(c,l) &= c_1 f(x,y) + c_2 f(x+1,y) \\ &+ c_3 f(x,y+1) + c_4 f(x+1,y+1) \end{aligned} \tag{10}$$

where c_i are the weighting values defined as follows:

$$\begin{aligned} c_1 &= (1+\Delta x)(1-\Delta y) \\ c_2 &= \Delta x(1-\Delta y) \\ c_3 &= (1+\Delta x)\Delta y \\ c_4 &= \Delta x \Delta y \end{aligned} \tag{11}$$

Cubic convolution resampling considers the DNs of the 16 nearest pixels, which improves the visual aspect but requires high computing capacity (Gibson and Power, 2000). This method uses third-order bivariate procedures. The 16 pixels involved are averaged according to distance and then linearly interpolated in groups of four lines with four pixels in order to create four interpolants. Then, another linear interpolation is performed between the four values obtained. The result of this process constitutes the transferred DN.

The expression for the one-dimensional interpolation as a function of the four values in a line is the following:

$$\begin{aligned} f(l) = \Delta x\{&\Delta x(\Delta x[f(x+2) - f(x+1) + f(x) - f(x-1)] \\ &- [f(x+2) - f(x+1) + 2f(x) - 2f(x-1)]) \\ &+ [f(x+1) - f(x-1)]\} + f(x) \end{aligned} \tag{12}$$

which, expressed as a function of the luminances of each cell, gives:

$$\begin{aligned} f(l) = &[(\Delta x)^3 - (\Delta x)^2]\, f(x+2) \\ &- [(\Delta x)^3 - (\Delta x)^2 - (\Delta x)]\, f(x+1) \\ &+ [(\Delta x)^3 - 2(\Delta x)^2 + 1]\, f(x) \\ &- [(\Delta x)^3 - 2(\Delta x)^2 - (\Delta x)]\, f(x-1) \end{aligned} \tag{13}$$

where $f(l)$ is the interpolant assigned to the central cell (l) of each of the four lines in the corrected image, and $f(x)$ is the value of the output image pixel located in the position defined by the real number.

The interpolating polynomial between the four $f(l)$ values obtained is expressed as:

$$\begin{aligned} f(c,l) = &[(\Delta y)^3 - (\Delta y)^2]\, f(l+2) \\ &- [(\Delta y)^3 - (\Delta y)^2 - (\Delta y)]\, f(l+1) \\ &+ [(\Delta y)^3 - 2(\Delta y)^2 + 1]\, f(l) \\ &- [(\Delta y)^3 - 2(\Delta y)^2 - (\Delta y)]\, f(l-1) \end{aligned} \tag{14}$$

Different methods can be used to resample the corrected image, and all of them alter the DNs of the new image more or less severely. Figure 8 shows the result of the resampling process for the three methods. The pixels involved in each resampling method are plotted in three levels of gray.

With regard to the contribution of the thermal band, the influence of the thermal band on the maximum likelihood method was verified by reclassifying the images without using the infrared record.

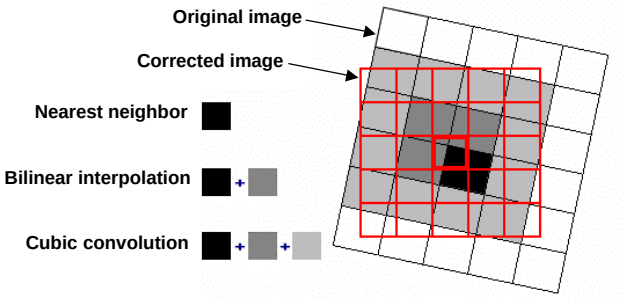

Figure 8. Resampling methods.

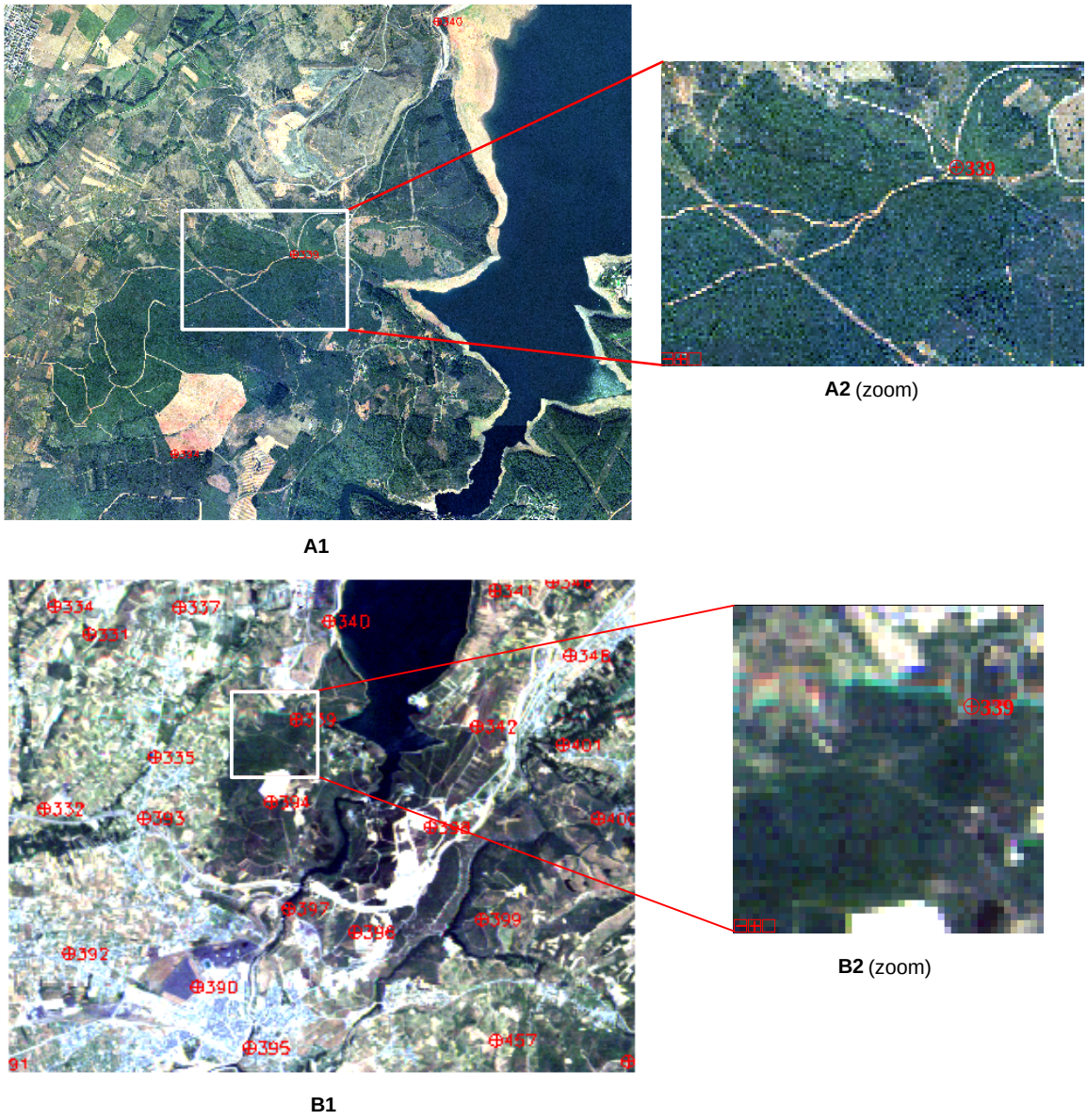

Figure 9. Detail of training areas.

Phase 4: Combination of Classified Images to Improve Results of Initial Classification

The images acquired in June and September and classified by using the maximum likelihood algorithm were combined. In the combined image, each pixel was assigned a cover type if, and only if, the informational class coincided in both images. Consequently, the pixels that were classified as vineyard in the combined image were also classified as vineyard in the images from June (image I) and September (image II). Unclassified pixels corresponded to pixels assigned to different cover types in images I and II. The classifications of images I and II were combined either directly or converted to vector format.

Phase 5: Estimation of Area under Vines by Correlating Results with Statistical Data

From among the different classifications conducted, the most accurate classifications were determined by using confusion matrices. Two validation methods were used: systematic sampling, and plot sampling.

The sampling unit used in the first validation method was the pixel. The sample size was calculated for 95% confidence (z = 1.96), with a maximum acceptable error (ε) of 5%, and assuming 50% probability of success/failure (p = q). As a result, the number of pixels that had to be sampled (n) was:

$$n = \frac{z^2_{a/2}}{4\varepsilon^2} = \frac{1.96^2}{4(0.05)^2} = 385 \qquad (15)$$

In order to guarantee the representativeness of the validation pixels, a simple random sampling was designed by developing a 700 × 700 m grid that covered all the municipalities included in the Designation of Origin "Bierzo." Two ground truth images were generated from this grid, based on the characteristics of the two images studied. Therefore, the sampling pixels for images I and II were the same, which enabled comparison of results. The pixel size generated using ENVI software was 28 × 28 m.

A second validation was carried out by using sampling areas (plots) selected by the classifier. These plots were

located in zones with homogeneous cover that were representative of the whole study area.

A confusion matrix was used to measure overall classification accuracy, user's and producer's accuracy, kappa statistic (κ), etc. In the confusion matrix, each cell contained a number that represented the amount (or percent) of pixels in the sample that, although belonging to row class in the classified image, was shown to belong to column class by actual verification. The accuracy of the classification increases with the increase in the values contained in the major diagonal as compared to the rest of the values. Non-diagonal errors represent classification errors of two types: (1) omission errors: column residuals show cover types that have not been correctly assigned to their class (type I error), and (2) commission errors: the elements included in the same row represent pixels that were assigned to a category while belonging to another (type II error). This type of error can be observed in row residuals.

Results and Discussion

In regard to the pre-processing phase, 557 ground control points (GCP) were used to correct the geometric distortions of image I (25 June 2000), and 475 control points were used in the case of image II (5 Sept. 2000). A better fit was obtained for image II, with a root mean square error (RMSE) of 0.670010 (fig. 9).

According to spectral analysis, the longest wavelength bands were the most heterogeneous bands in both images, except for band 6, which was the most homogeneous band, and band 4 in image II, with a maximum value of 178. The range of variation of the visible bands was very wide but deviations were small, which suggests a clustering of the DN values around the mean.

With regard to image classification, visual interpretation showed that the most recent vineyards covered larger areas. However, these vineyards were confused with bare soil or new forests due to trellis training and scarce vine development. In general, the colors that characterized vineyards were similar to the colors of agricultural land before harvest. Image II, acquired in September, showed darker and more intense colors than image I, acquired in June, due to the differences in cover, vigor, and atmospheric conditions. Table 1 shows the 18 classes identified by using the training areas. The final classes were obtained after reorganization of the initial 38 discriminated cover types.

Training areas were defined on the images so that these areas were as representative as possible. A sufficient number of plots were defined for each class in order to cover the different types of slope, orientation, elevation, density, vigor, etc. Moreover, the training sites selected showed the same location in both images in order to allow for comparison of classifications.

The use of classification algorithms showed that the visual appearance of all the classified images was very similar, except for parallelepiped classification, in which the pixels assigned to the cover types "vineyard" and "other unproductive land" prevailed. This type of classification yielded the poorest results. The classifications obtained by using minimum distance and Mahalanobis distance were very similar. However, in the minimum distance classification, the pixels assigned to agricultural crops prevailed, while the Mahalanobis classification showed an increase in the forested cover. These trends were maintained in the classifications obtained for image II.

In image I, the vineyard area estimated with minimum distance classification exceeded by more than 100 ha the vineyard area estimated with Mahalanobis distance classification. The comparison of these classifications with the image from September yielded differences of more than 1900 ha.

The two images were classified by using the maximum likelihood method and resampled according to the two approaches considered. The differences between the areas obtained for each cover type depended on the season in which the images were acquired rather than on the resampling method. The largest differences were observed for the cover types "bracken" and "conifers," which covered 2500 ha less with cubic convolution resampling. In the image from September, the most relevant changes were observed for the cubic convolution method, and mainly for agricultural crops.

Table 1. Definition of the discriminated land cover types.

Class	Cover Type	Description
1	Irrigated cropland	Agricultural land that shows evidence of some irrigation system.
2	Rainfed cropland	Agricultural land used for rainfed crops. Fallow land and abandoned crops are included in this cover type.
3	Grasslands	Irrigated or rainfed areas covered by herbaceous species and used for grazing or mowing.
4	Bracken	Areas covered by bracken.
5	Pasture	Herbaceous pastures with less than 20% cover of small shrub and/or trees.
6	Shrubland	Sub-shrubs (thyme, true lavender, etc.) and shrubs (strawberry tree, broom, gum rockrose, etc.).
7	Shrubland with trees	Shrubland areas with less than 30% cover of trees.
8	Forest: broadleaf	Forested areas with more than 60% cover of chestnut, common oak or evergreen oak.
9	Forest: riparian	Areas near water courses with cover of poplar, alder tree and other riparian vegetation.
10	Forest: conifers	Reforested areas with more than 70% cover of conifers.
11	New forests	Recently reforested areas with less than 30% cover of forest.
12	Bare land	Areas with bare soil prepared for reforestation, rocky areas, clearings, and dumps.
13	Urban and roads	Spaces structured into built-up areas (continuous or discontinuous), streets and road networks.
14	Other unproductive land	Industrial areas, dumps, stockpiles of material, etc.
15	Water	Reservoirs for water storage and water courses.
16	Vineyard: trellis	Recently planted vines or vines trained on a trellis, covering less than 20% of soil during the maximum growth period.
17	Vineyard: wide spacing	Adult vineyards with low planting density that cover less than 60% of soil during the maximum growth period, or vineyards that have not reached maximum growth.
18	Vineyard: close spacing	Adult vineyards with low planting density that cover up to 60% of soil during the maximum growth period.

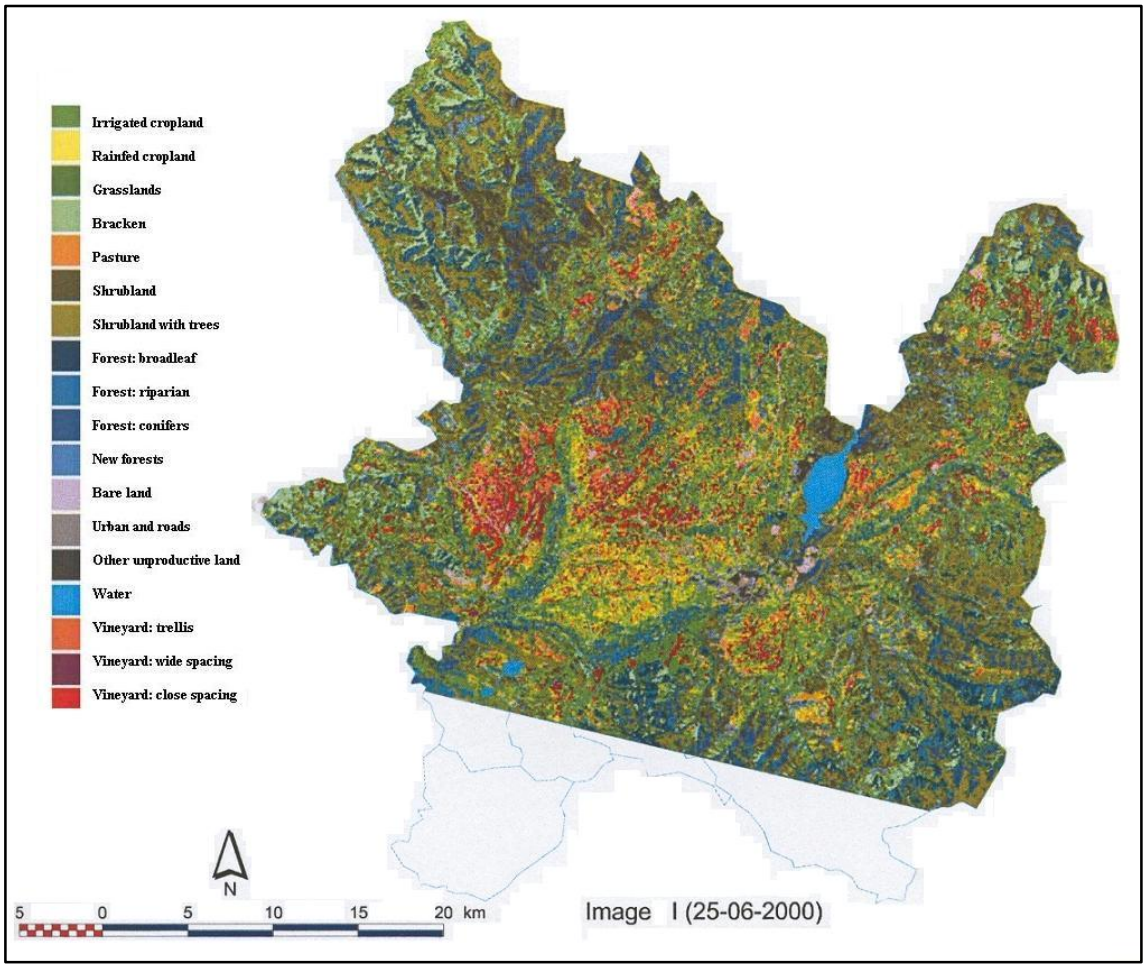

Figure 10. Example of classification for image I.

Table 2. Area (ha) of each cover type according to the classification algorithm used (image I).

Cover Type	Parallelepiped	Minimum Distance	Mahalanobis Distance	Maximum Likelihood	
				Cubic Convolution	Nearest Neighbor
Irrigated cropland	0.00	10231.51	8609.88	9270.87	7133.38
Rainfed cropland	0.00	9271.42	5707.36	7710.87	7065.17
Grasslands	59.11	4847.23	6745.30	7393.66	5479.21
Bracken	42.80	8495.42	7757.28	3078.84	5561.06
Pasture	51.97	3359.04	4031.48	3096.01	3820.74
Shrubland	5.33	9052.76	8527.72	10332.33	8392.64
Shrubland with trees	0.00	24705.48	26798.68	15920.06	16270.50
Forest: broadleaf	1629.54	12157.33	15384.98	22806.63	23288.95
Forest: riparian	816.37	7272.69	5034.06	4746.88	5934.25
Forest: conifers	378.75	8832.70	9383.46	8600.40	11616.76
New forests	448.36	10638.88	10680.74	9582.51	7932.27
Bare land	5521.63	1182.82	1338.44	3558.81	3499.93
Urban and road	18469.55	1447.34	2084.10	4882.43	4942.57
Other unproductive land	62586.40	2953.95	2287.47	3921.80	3673.90
Water	626.65	1059.81	1034.95	809.32	858.55
Vineyard: trellis	1004.46	2457.99	1978.03	1142.99	1569.33
Vineyard: wide spacing	12850.54	5058.83	4491.14	5068.32	3589.54
Vineyard: close spacing	21049.38	3146.03	4296.16	4248.49	5542.48
Unclassified	630.41	0.00	0.00	0.00	0.00
Total area under vines	34904.38	10662.85	10765.33	10459.8	10701.35
Total	126171.31	126171.32	126171.32	126171.32	126171.32

The areas under vines obtained with the maximum likelihood algorithm were similar for both resampling methods. However, the results of the classifications obtained by using the image acquired in September were much higher. Figure 10 and table 2 show the results obtained for image I.

In regard to the effects of the different factors, we first considered the resampling method. The DNs of the original image were transferred to the corrected image by a resampling process. Nearest neighbor and cubic convolution were used. The nearest neighbor method was used because it was the approach that least distorted the original DN values (Pinilla, 1995). The results obtained for the different resampling and classification methods used are jointly presented and discussed further in this section.

Contrary to what was expected, the results obtained for the contribution of thermal bands to maximum likelihood classification showed significant variation when thermal bands were excluded from the classification. The most remarkable changes affected the cover types "grasslands," "forest," and "other unproductive land." However, these changes hardly affected the areas assigned to vines. In the image from June, the area under vines increased by 28 ha, while in the image from September, the area under vines increased by 18 ha. These results revealed a decrease in the accuracy levels, but such a decrease was not relevant. Therefore, the use of the thermal band contributed to improving the accuracy of the maximum likelihood classification conducted.

By combining the images from June and September, large differences were observed in data for "shrubland with trees" (more than 4200 ha) and "other unproductive land" (more than 1200 ha). The area assigned to vineyards with this methodology amounted to 3200 ha in the case of the image from June and 3500 ha in the case of the image from September, while the actual area covered by this crop in El Bierzo accounts for about 7000 ha.

The results obtained for the images classified by using the maximum likelihood algorithm were combined. The confusion matrix obtained by overlaying the image from September on the image from June revealed a considerable increase in overall accuracy and a decrease in errors of commission and omission, as expected. However, many pixels that were not assigned to the same cover type in both images were lost. The highest producer's accuracy corresponded to the vineyards with the lowest planting density, and trellised vines showed the lowest error of commission. The results obtained by overlaying the image acquired in June on the image acquired in September showed little variation. As in the previous case, the main errors were caused by confusion of vineyards with grasslands.

The combination of both images caused a decrease in the number of classified pixels. However, the overall classification accuracy increased up to more than 54%. With regard to vineyard cover, user's accuracy increased up to 86% to 92%, and errors of commission decreased to 35% to 34%.

Images I and II were combined after conversion to vector format. The results were similar to the results obtained with raster combination, but the value of the kappa statistic increased up to 0.50 to 0.49. Conversely, errors of commission increased when each vineyard type was considered separately. In this type of combination, the percentage of agreement improved considerably, errors of omission and commission decreased, and sampling errors increased because fewer classified pixels were used for validation.

After combining the classifications of the images from June and September, either directly or converted to vector format, wide areas remained unclassified: 80,000 ha for the combinations based on the classifications of the image from June, and 77,000 ha for the image from September.

Systematic Sampling Validation Method

This section presents the validation results obtained for the systematic sampling method, which provides statistical robustness. However, systematic sampling works with individual pixels and does not consider the surrounding pixels, which can be a problem in zones with highly fragmented and heterogeneous covers, as in the case of El Bierzo. In other words, in highly tessellated areas, a DN value often corresponds to more that one cover, unless the pixel is located within a uniform tile that is larger than the spatial resolution of the sensor (30 m for Landsat images).

Each type of classification was validated by crossing the ground truth images with the classified images. Because the best values were obtained with maximum likelihood classifications, the results of these classifications are presented below.

Table 3 shows the results obtained for the image acquired in June. These results suggest that accuracy depended on the resampling method used. Although similar values were obtained with both methods, a higher accuracy value was obtained with cubic convolution than with nearest neighbor. In general, overall accuracy values were low. Better accuracy values were obtained for vineyards as compared to previous classifications, but overestimation of the areas under vines still occurred, with considerable errors of commission. Table 4 shows the confusion matrix for the image acquired in June, resampled by using the cubic convolution method. Errors derive from the confusion of vineyards with agricultural areas, grasslands, and shrubland with trees.

In the case of nearest neighbor resampling, errors occurred in agricultural areas, grasslands, and forests, and confusion increased in pasture areas and pure shrub covers. With regard to accuracy, the vineyards that were best identified by the user were widely spaced vineyards (21.33%), while the vineyards best identified by the producer were vineyards with high planting densities (37.77%).

The confusion matrices for the image acquired in September revealed errors in the classification of vineyard covers, which were confused with shrubland, and with agricultural and farming covers. In addition, there was an increase in the error of commission, caused by the vineyards with the highest planting densities.

The maximum likelihood algorithm improved the accuracy of the classifications. However, the accuracy levels obtained were considerably low. A possible explanation for

Table 3. Effect of the resampling method on the classification (image I).

	All Covers				Vineyard Covers			
					Accuracy		Error	
Maximum Likelihood	Overall Accuracy	Sampling Error	Confidence Interval	Kappa	Producer	User	Omission	Commission
Cubic convolution	36.23	0.9502	1.862	0.2961	73.33	39.63	26.67	60.37
Nearest neighbor	32.99	0.9294	1.822	0.2617	65.83	37.26	34.17	62.74

Table 4. Summarized confusion matrix for maximum likelihood classification (image I using cubic convolution).

Class	1	2	3	4	5	6	7	8	9	10	11	12	13	14	15	16	17	18	Total	User's Accuracy
1	28	18	28	0	10	12	45	10	9	3	6	1	10	0	0	1	3	4	188	14.89
2	29	32	28	0	13	17	13	1	1	0	6	2	6	0	0	1	5	3	157	20.38
3	7	11	58	1	23	4	28	11	2	0	0	1	0	0	0	0	0	5	151	38.41
4	2	0	11	4	4	2	21	20	1	0	0	0	0	0	0	0	0	0	65	6.15
5	3	11	6	0	17	9	3	0	0	0	2	3	0	0	0	3	1	0	58	29.31
6	3	2	1	0	15	100	29	10	4	13	25	4	0	0	1	0	0	0	207	48.30
7	2	2	8	0	15	77	107	77	8	17	7	1	0	0	0	0	0	0	321	33.33
8	0	0	11	2	8	12	80	308	24	18	2	0	0	0	0	0	0	0	465	66.23
9	1	0	3	0	1	0	10	33	36	7	0	0	0	0	0	0	0	0	91	39.56
10	0	0	1	0	1	31	38	38	3	48	6	0	0	0	0	0	0	0	166	28.91
11	5	3	8	0	27	40	28	8	2	3	49	7	7	1	0	0	0	1	189	25.92
12	3	4	3	0	7	4	1	1	0	3	5	30	20	0	0	3	0	0	84	35.71
13	4	3	6	0	3	7	3	1	1	3	2	7	45	1	1	0	2	0	89	50.56
14	0	0	3	0	7	32	20	8	0	5	3	5	2	5	0	0	0	0	90	5.55
15	0	0	0	0	0	0	0	0	0	0	0	0	0	0	16	0	0	0	16	100.00
16	3	4	0	0	1	0	0	0	0	0	1	4	0	0	0	7	5	4	29	24.13
17	10	15	13	0	3	6	9	0	0	1	2	2	2	0	0	1	23	14	101	22.77
18	7	9	23	1	8	2	7	0	0	0	0	1	0	0	0	0	20	14	92	15.21
Total	107	114	211	8	163	355	442	526	91	121	116	68	92	7	18	16	59	45	2559	
Producer's accuracy	26.16	28.07	27.48	50.00	10.42	28.16	24.20	58.55	39.56	39.66	42.24	44.11	48.91	71.42	88.88	43.75	38.98	31.11		

low accuracy levels is the high fragmentation of the covers and the loss of accuracy in the geographical location of the pixels that composed the ground truth images.

Plot Sampling Validation Method

Table 5 summarizes the number of plots sampled, the number of pixels, and the area of each cover type in both images. In the validation images, a total of 65 plots under vines with a mean surface area of 4000 m^2, which corresponds to five pixels, were sampled. These figures suggested that confusion matrices would contain approximately 1800 pixels (about 140 ha) assigned to vineyards.

As in the case of systematic sampling, the plot sampling validation method estimated the influence of the resampling method and of thermal bands on maximum likelihood classification. The analysis of the results obtained for the images acquired in June and September suggested that the sampling method used for geometric correction affected the results of the classification. The use of plot sampling (targeted sampling) yielded much higher accuracy levels than the use of systematic sampling.

The overall accuracy obtained for the image acquired in June amounted to almost 80% with cubic convolution and 75% with nearest neighbor. Considering the vineyards as a whole, user's accuracy and producer's accuracy increased by five percentage points (on average) with cubic convolution as compared to nearest neighbor resampling (table 6). The improvement in validation results became very evident in the analysis of the confusion matrices. The confusion of vineyards with herbaceous crops was lower in the case of cubic convolution, as compared to nearest neighbor. Another source of error in the classification derived from the confusion of bare land with recently planted vines, usually trained on a trellis. Type II vineyards showed considerable errors with both resampling methods. However, confusion was observed mainly in type III vineyards, which were very dense. The accuracy of the vineyard cover considered as a whole was not severely affected.

Table 5. Characteristics of ground truth images (validation plots).

Cover	No. of Plots	Image I (25 June 2000) Pixels	Image I (25 June 2000) Area (ha)	Image II (5 Sept. 2000) Pixels	Image II (5 Sept. 2000) Area (ha)
Irrigated cropland	117	628	49.23	629	49.31
Rainfed cropland	64	469	36.76	474	37.16
Grasslands	155	644	50.48	643	50.41
Bracken	17	29	2.27	38	2.97
Pasture	95	1075	84.28	1070	83.88
Shrubland	95	665	52.13	656	51.43
Shrubland with trees	34	227	17.79	236	18.5
Forest: broadleaf	241	1990	156.01	1993	156.25
Forest: riparian	131	761	59.66	767	60.13
Forest: conifers	102	929	72.83	938	73.53
New forests	71	532	41.7	538	42.17
Bare land	107	867	67.97	863	67.65
Urban and roads	132	845	66.24	850	66.64
Other unproductive land	62	404	31.67	415	32.53
Water	26	5906	463.03	5895	462.16
Vineyard: trellis	55	393	30.81	391	30.65
Vineyard: wide spacing	102	491	38.49	479	37.55
Vineyard: close spacing	208	917	71.89	922	72.28
Total	1814	17772	1393.24	17797	1395.20

With regard to the classification based on the image from September, good results were obtained, with kappa values higher than 0.70. Errors of omission (15% to 19%) and commission (20% to 24%) for vineyards were maintained within an acceptable range. In the confusion matrices for September, some pixels that corresponded to sparse evergreen oaks (included in the land cover "broadleaf forests") were classified as vines. These results confirm the results obtained by using systematic sampling: the cubic convolution resampling method improves the accuracy of the maximum likelihood classification.

With a view to assessing the contribution of the thermal band to the classification, the images were reclassified by

Table 6. Effect of the resampling method on image II (validation plots).

Maximum Likelihood	All Covers				Vineyard Covers			
					Accuracy		Error	
	Overall Accuracy	Sampling Error	Confidence Interval	Kappa	Producer	User	Omission	Commission
Cubic convolution	79.43	0.3032	0.594	0.7598	89.95	85.98	10.05	14.02
Nearest neighbor	74.79	0.3257	0.638	0.7057	84.95	81.03	15.05	18.97

Table 7. Influence of the use of the thermal band on the classification (validation plots).

Maximum Likelihood	All Covers				Vineyard Covers			
					Accuracy		Error	
	Overall Accuracy	Sampling Error	Confidence Interval	Kappa	Producer	User	Omission	Commission
June (6 bands)	78.41	0.3086	0.605	0.7479	88.72	85.59	11.28	14.41
September (6 bands)	77.25	0.3142	0.616	0.7347	82.42	79.23	17.58	20.77

using bands 1, 2, 3, 4, 5, and 7. When validation was carried out by using validation plots, the following overall results were obtained: Accuracy decreased by one or two percentage points as compared to the classification of the images resampled with cubic convolution. However, accuracy increased as compared to the nearest neighbor classification of the images (table 7). Kappa values decreased from 0.7598 to 0.7479 for the image acquired in June and from 0.7611 to 0.7347 for the image acquired in September. Therefore, it can be stated that the thermal band provides useful information for the maximum likelihood algorithm.

The analysis of the confusion matrices revealed that the main errors (relevant to this research) occurred due to confusion of vineyards with agricultural and farm uses. In the classification of the image from June, there was an increase in the number of pixels that corresponded to "pasture" and were classified as "vineyard." In the case of September, an increase occurred in the "broadleaf forest" pixels that were classified as "vineyard." The main errors of omission in vineyards (larger than 60%) were caused by confusion between cover types 17 and 18 (both of them "vineyard" classes). In this case, errors of commission exceeded 50% due to this type of confusion in the classification.

Like in the previous validations, the accuracy of the combination of the two classified images was determined by using the maximum likelihood algorithm. Again, the best results were obtained with the combination of the images acquired in June and September. The overall accuracy rate was about 94%, and the producer's accuracy for the three types of vineyards exceeded 97%, while the user's accuracy was 94%.

The analysis of the complete confusion matrices suggested that good results were maintained. The most remarkable errors obtained with the combination based on image I were: classification of 14 pixels that corresponded to trellis vines as "pasture," classification of 14 pixels that were (in all likelihood) fruit orchards as irrigated crops, and classification of 42 "bare land" pixels as trellis vines.

The verified pattern was confirmed by conducting the combination based on the image from September. The producer's accuracy obtained for the classification of trellis vines was 88.14%, and the error of commission was 15.91%. For widely spaced vines, the user's accuracy and the producer's accuracy decreased to 76.68% and 57.81%, respectively. Closely spaced vines were classified with an error of omission of 4.56% and an error of commission of 14.89%.

The accuracy levels were maintained when the combination of images was carried out by converting classifications to vector format for subsequent rasterization. Kappa values of 0.9065 and 0.8991 were obtained for the combinations based on the images from June and September, respectively. The partial results obtained for each type of vineyard were maintained.

By combining the images that were classified without considering the thermal band, producer's accuracy exceeded 96% and user's accuracy reached 93.31%. With the plot sampling method, the confusion of vineyards with agricultural and farming covers decreased considerably. However, the confusion between vineyards with high planting densities and vineyards with low planting densities was maintained.

Although many unclassified pixels were lost in this validation, the sampling errors increased less than in validations conducted by using a random grid, in which the number of sampling areas was considerably lower.

The last part of this study focused on determining the relationship between the results obtained and the statistical data available. Table 8 shows the areas under vines estimated for each municipality, specifically the areas estimated using the maximum likelihood algorithm and combining the two

Table 8. Estimated and actual areas under vines in the different municipalities.

Municipality	Vector Combination (ha)		New Register JCyL (2003) (ha)
	June	September	
Arganza	229.71	260.84	562.06
Bembibre	43.67	53.86	78.21
Borrenes	52.99	54.88	103.23
Cabañas Raras	129.98	144.09	289.67
Cacabelos	397.88	429.87	976.36
Camponaraya	446.64	492.19	1110.17
Carracedelo	99.96	112.50	207.12
Carucedo	6.97	7.68	20.09
Castropodame	70.09	75.11	108.85
Congosto	72.99	86.71	123.7
Corullón	127.87	145.04	219.41
Cubillos + Fresnedo	90.79	105.06	7.64
Molinaseca	24.38	25.72	65.73
Ponferrada	501.37	547.78	1402.06
Priaranza del Bierzo	27.98	27.05	138.96
Sancedo	63.19	74.56	152.49
Vega de Espinareda	119.79	138.21	18.81
Villadecanes	239.98	261.54	520.11
Villafranca del Bierzo	468.67	502.62	1112.88
Bierzo total	3277.12	3612.28	7322.37

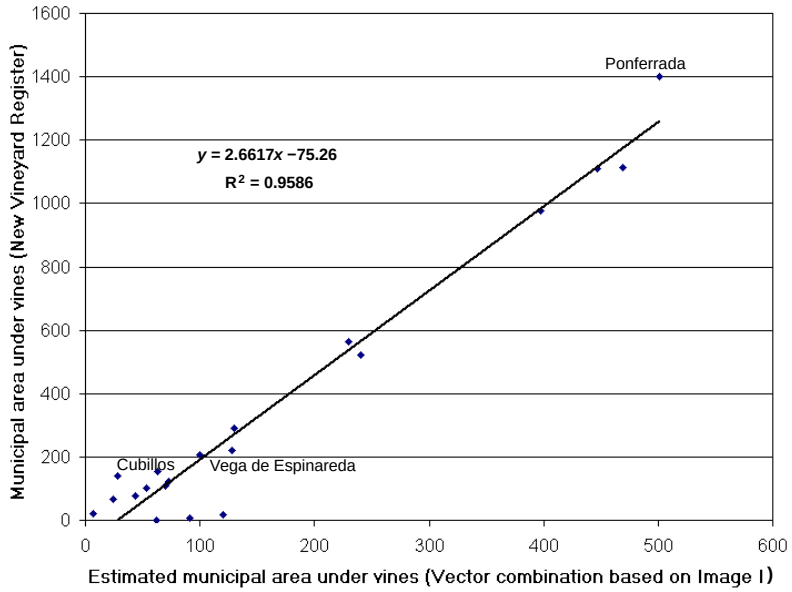

Figure 11. Linear regression between the New Vineyard Register of Castilla y León and the combination of vector images based on the image from June.

images converted to vector format (vector combination). Considerable differences can be observed between the classification of the image acquired in June and the classification of the image acquired in September because of the different conditions under which the images were acquired. The last column shows updated information about the area under vines in El Bierzo. This information corresponds to the new Vineyard Register of Castilla y León (VRCyL), compiled in 2002.

Table 8 shows very large differences between the data obtained from our classification and the statistical source consulted. Nevertheless, the correlations between the data obtained in this study and the official statistical data were determined by verifying their statistical significance. The regressions of the relationship between the statistical data contained in the VRCyL and the combinations of the images converted to vector format exceeded 95%. To complement regression, the linear equations obtained in the fit (for the best result obtained) are presented in figure 11.

The regression lines for the relationship between the vineyard areas estimated from the image acquired in September and the data from the new VRCyL yielded the poorest results. The area under vines was overestimated for some municipalities in which shrubland prevailed (Vega, Corullón, etc.). However, the estimations for other municipalities such as Cacabelos or Camponaraya were more approximate but deviated from the line due to the poor fit caused by the distortions mentioned above. The best regression was obtained by relating the information from the VRCyL and the result of combining the two classifications in vector format, based on image I. Figure 11 shows this regression. Despite the good fit obtained, the underestimation of the area under vines due to the small size of vineyards was very evident. Underestimation caused transfer of an error in the classification of one pixel to this combination.

Poor spatial resolution, as in the case of the imagery used in this study, can cause occurrence of mixed signals from two or more covers in the same pixel; excessive bandwidth or an insufficient number of bands may neglect some differences. Moreover, in regard to temporal resolution, data collected in the same season of the year can lead to confusion between covers in particular moments of their phenological development (Chuvieco, 2002).

CONCLUSIONS

Considering the need for reliable and timely statistical information on vineyards, remote sensing can be used as a tool to map and estimate vineyards in a fast and efficient manner, so that such information is available for decision making in key moments. The use of satellite imagery as a tool to determine cultivated areas offers a fast and economic method to acquire data.

After comparing the most widely used classification methods, the method that yielded the best results for the identification of vineyards in the Designation of Origin "Bierzo" was the maximum likelihood algorithm. Moreover, the most correct vineyard classifications were obtained by using the image from June due to the higher vegetative vigor of vines, which enabled better identification of vines in that season.

The best validation results for the classifications conducted were obtained by distributing plots with targeted sampling.

The resampling method affected classification accuracy. However, the incidence of this factor was not very relevant. The results obtained for both images suggest that the cubic convolution approach is more appropriate than the nearest neighbor approach.

Within the geographical framework of study, and for the images used, the use of thermal bands in the classification contributed to improving overall and specific accuracy of vineyard classification.

The two classified images were combined to improve accuracy. The pixels classified as vineyard in the combined image coincided with the pixels classified as vineyard in each individual image. By combining the images, the kappa statistic of the classification improved considerably, but the number of unclassified pixels increased.

The data obtained from the classification showed a strong correlation with the most reliable statistical data available on vineyard areas at the municipal level. Such strong correlation contributed to establishing linear regressions that enabled estimation of the municipal area under vines based on the classifications.

In view of the results obtained, we can conclude that the use of Landsat TM imagery is appropriate to record overall variations in the study area every three years. The proposed method can replace the field sampling method currently used to update vineyard registers. However, the accuracy of this type of sensing technique is inadequate to compile inventories that require detailed classification of land uses. Sensors with higher spatial resolution should be used for this purpose.

REFERENCES

Arán, M., P. Villar, J. Xandri, L. Albizua, A. Leránoz, M. Zalba, and X. Farré. 2001. Estudio de las relaciones entre las propiedades del suelo, cubierta vegetal y respuesta espectral en el cultivo de la viña. In *Teledetección: Medio Ambiente y Cambio Global*, 29-32. J. I. Rosell Urrutia and J. A. Martínez-Casasnovas, coords. Lleida, Spain: Universitat de Lleida and Editorial Milenio.

Bessa, M. J. 1994. Methodologie pour la carthographie des surfaces occupees par la vigne et macrozonage des potentiales viticoles dans la region delimite du Douro. In *Proc. 5th European Conference and Exhibition on Geographical Information Systems − ESRI GIS.* Paris, France. Available at http://libraries.maine.edu/Spatial/gisweb/spatdb/egis/eg94067a.html.

Bugden, J. L., G. Salinas de Salmuni, and P. J. Howarth. 1999. RADARSAT Vineyard identification in the Tulum Valley, Argentina. In *Proc. 4th International Airborne Remote Sensing Conf. and Exhibition, 21st Canadian Symp. on Remote Sensing*, 375-382. Ottawa, Canada: Canadian Remote Sensing Society.

Chuvieco, E. 2002. *Teledetección Ambiental: La Observación de la Tierra desde el Espacio*. Barcelona, Spain: Editorial Arie.

Company, A., G. Delpont, S. Guillobez, and M. Arnaud. 1994. Potentiel des données radar ERS-1 pour la détection des surfaces contributives au ruissellement dans les vignobles méditerranéens du Roussillon (France). In *6eme Symposium International Mesures Physiques et Signatures en Télédétection*, 375-382. Val d'Isère, France.

Eastman, J. R. 1999. IDRISI 32 tutorial. Worcester, Mass.: Clark University, Clark Labs.

Escalera, A. de la. 2001. *Visión por Computador. Fundamentos y Métodos*. Madrid, Spain: Pearson Educación.

Franson, P. 2001. Napa grapes seem from space: Remote sensing proving long-term value in vineyards. Available at: www.traveltastes.com/remote%20sensing.htm.

García, J. S., and F. M. García. 2001. Evolución de la superficie ocupada por viñedo en La Mancha Conquense en la última década: Aplicación con la imagen Landsat. In *Teledetección: Medio Ambiente y Cambio Global*, 61-64. J. I. Rosell Urrutia and J. A. Martínez-Casasnovas, coords. Lleida, Spain: Universitat de Lleida and Editorial Milenio.

Gibson, P., and C. Power. 2000. *Introductory Remote Sensing: Digital Image Processing and Applications.* New York, N.Y.: Routledge.

Hall A., D. W. Lamb, B. Holzapfel, and J. Louis. 2002. Optical remote sensing applications in viticulture: A review. *Australian J. Grape and Vine Res.* 8(1): 36-47.

Lanjeri, S. 1998. Análisis mediante teledetección de los cambios en el uso agrícola del suelo relacionados con el viñedo en zonas amenazadas de desertificación en Castilla-La Mancha. MS thesis. Valencia, Spain: University of Valencia.

Lanjeri, S., J. Melia, and D. Segarra. 2001a. A multitemporal masking classification method for vineyard monitoring in central Spain. *Intl. J. Remote Sensing* 22(16): 3167-3186.

Lanjeri, S., J. M. Royo, D. Segarra, and J. Meliá. 2001b. La evolución interanual del cultivo del viñedo en Castilla-La Mancha (1991-2000) analizada con imágenes Landsat. In *Teledetección: Medio Ambiente y Cambio Global*, 118-122. J. I. Rosell Urrutia and J. A. Martínez-Casasnovas, coords. Lleida, Spain: Universitat de Lleida and Editorial Milenio.

Lillesand, T. M., and R. W. Kiefer. 1994. *Remote Sensing and Image Interpretation.* 3rd ed. New York, N.Y.: John Wiley and Sons.

Martínez, J., J. R. Rodríguez, and A. Fernández. 2002. La teledetección como herramienta para la ordenación rural sostenible en entidades locales menores. In *Actas del X Congreso de Métodos Cuantitativos, Sistemas de Información Geográfica y Teledetección*, CD-ROM. Valladolid, Spain: Universidad de Valladolid, Spain.

Pinilla, C. 1995. *Elementos de Teledetección.* Madrid, Spain: Ra-Ma Editorial.

Ranchin, T., B. Naert, M. Albuisson, G. Boyer, and P. Astrand. 2001. An automatic method for vine detection in airborne imagery using wavelet transform and multiresolution analysis. *Photogrammetric Eng. and Remote Sensing* 67(1): 91-98.

Robbez-Masson, J. M., T. Wassenaar, P. Andreux, F. Baret. 2001. Reconnaissance par télédétection rapprochée des vignes et analyse de leur structure spatiale á l'aide d'une analyse fréquentielle intra-parcelaire. Application au suivi effect des pratiques culturales. *Ingénieres* 27: 59-69.

Rodríguez, J. R. 2003. Teledetección mediante imágenes de satélite. Aplicación para la localización de viñedos en la DO Bierzo. PhD diss. Lugo, Spain: University of Santiago de Compostela, Department of Agricultural and Forestry Engineering.

Rodríguez, J. R., F. Riesco, and C. J. Álvarez. 2002. Aplicación de la teledetección a la inventariación de viñedo en la zona de Denominación de Origen Bierzo. In *Actas del XIV Congreso Internacional de Ingeniería Gráfica*, 424-433. Santander, Spain: University of Cantabria.

RSI. 2000. ENVI tutorials. Boulder, Colo.: RSI.

Rubio, E., M. M. Artigao, V. Caselles, C. Coll, and E. Valor. 2001a. Cartografiado de la vid con datos Landsat TM. Aplicación a una zona de Tomelloso (Ciudad Real). *Revista de Teledetección* 15: 47-56.

Rubio, E., M. M. Artigao, V. Caselles, C. Coll, and E. Valor. 2001b. Clasificación del viñedo en la zona de Tomelloso (Albacete). In *Teledetección: Medio Ambiente y Cambio Global*, 74-78. J. I. Rosell Urrutia and J. A. Martínez-Casasnovas, coords. Lleida, Spain: Universitat de Lleida and Editorial Milenio.

Trolier, L. J., W. R. Philipson, and W. D. Philpott. 1989. Landsat TM analysis of vineyards in New York. *Intl. J. Remote Sensing* 10(7): 1277-1281.

Tsiligirides, T. A. 1998. Remote sensing as a tool for agricultural statistics: A case study of area frame sampling methodology in Hellas. *Computers and Electronics in Agric.* 20(1): 45-77.

Wassenaar, T., F. Baret, J. M. Robbez-Masson, and P. Andreux. 2001. Sunlit soil surface extraction from remotely sensed imagery of perennial, discontinuous crop areas; the case of Mediterranean vineyards. *Agronomie* 21: 235-245.